Optica Applicata, Vol. XL, No. 4, 2010

Improved pores detection in fingerprints by applying ring led's (525 nm)

E.J. BUSSELAAR

Eindhoven University of Technology, epartment of Applied Physics,
Den Dolech 2, P.O Box 513, 5600 MB Eindhoven, The Netherlands

The requirement to determine the identity of a person is becoming more and more important in the present information society. There are a number of biometric based identification and verification systems on the market for many civilian, military and forensic applications. Amongst the reliable biometric systems, fingerprint authentication plays a major role, as fingerprints are not just related to criminality anymore. Several automated fingerprint identification or verification systems dictate the market and some apply pores as additional feature to the traditionally applied minutiae systems to improve the system performance. There is, however, a financial trade off between detection of pores and the complexity of the applied optical system. In this paper, the impact of using strike light and the application of a specific wavelength to improve the reflection on the skin is presented to improve the imaging performance of existing automated fingerprint identification or verification systems (AFIS or AFVS). The results are fingerprint images with distinct pores necessary for the image and feature processing. With the introduction of computers it became possible to automate data of fingerprints. The template (original) fingerprint images are compared with the live scan images, resulting in a match score. This match score is defined in terms of the number of false accepts and false reject errors and determines the performance of the system. Despite the inverse relation of these error rates, the lower both rates, the better the system. The final result of the introduced unique features is a system with error rates significantly better than with systems applying standard prism based white light sensors.
The application of all presently available fingerprint sensor systems has been extended significantly after the September 11-th incident.

Keywords: biometrics, fingerprint patterns for identification and verification, sensor design, applied telecentric optics, modulation transfer function (MTF) of an optical system, optical properties of the human skin, pores (Level 3) matching, system performance by statistical analysis (FAR and FRR analysis).

1. Introduction

The usage of fingerprints is going back long before Christ (BC). Its potential has been recognized only two centuries ago, when a Czech physiologist named Purkinje introduced a system of classifying fingerprints. He noted 9 different fingerprint patterns (level 1 qualification). In the 1880's, Sir Francis Galton, started his observations of fingerprints as a means of identification, establishing the individuality

and permanence of fingerprints. He recognised distinctive fingerprint features and quantified the uniqueness of fingerprints by conducting a probabilistic analysis of minutiae pattern. These features (minutiae) were qualified as level 2 (Galton) characteristics. In 1918 Edmond Locard wrote that if 12 points (Galton's details) were the same between two fingerprints, it would suffice as a positive identification. Subsequently, he studied the use of pores for identification (or poroscopy), and showed that 20 to 40 pores should be sufficient to establish human identity. With that phenomenon, he introduced level 3 features, which includes all dimensional attributes of a ridge, such as the shape, width, edge contour, breaks, creases, scars, and of course pores. ASHBAUGH [1] proved that level 1, 2 and 3 features are unique, permanent and immutable. JAIN *et al*. [2, 6, 7] observed a significant performance improvement (>20%), when level 2 (minutiae) matching is combined with level 3 (pores) matching, when high resolution sensors (≥800 dpi) are applied. It must be noted that level 1, 2 and 3 features are not independent within the domain of fingerprint identification and/or verification. A prototype has been designed to distinguish level 3 features.

2. Design considerations

All kinds of scanning methods have been developed to detect (or scan) a fingerprint. Most of these fingerprint sensors are optical sensors (prisms), solid state sensors (capacitive or thermal) and ultrasound sensors. There are only a few of these sensors which can cope with finger pad distortion analysis, whereby a high spatial resolution is required, as well as imaging through a non-flat contact surface. Prism based methodology can fulfil most of these requirements and is therefore the most frequently used method. The principle is as follows (ref. Fig. 1):

The system set up consists of a light source, a prism and a camera. The light wave hits both the contacted area as well as the non-flat contact area. When the light hits the surface, consisting of glass and air only, as shown in Fig. 1, the contact area reflects the light completely into the camera, resulting in a high contrast pattern of black ridges on a white background. This works according to the frustrated total internal reflection (FTIR) principle, which occurs when a ray of light strikes a medium

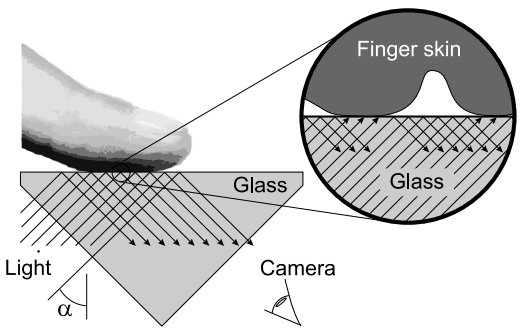

Fig. 1. Typical prism based automatic fingerprint sensor.

boundary at an angle larger than the critical angle with respect to the normal to the surface, whereby, in this case, the air is the "frustrated" medium. As the air film thinned out, near the ridges, the transition from total to almost no reflection occurs. Therefore, the non-flat area will absorb most of the light with some scattered light reflection. It is a relatively cheap methodology with no mechanical parts. In an ideal environment it will work satisfactory. However, there are a number of shortcomings to be mentioned:

1. Non-uniform contact; the ridge structure of the finger will be changed due to environmental conditions, outside temperature, dirt, sweat, air humidity, dryness of the skin and in time worn out ridges (special professions and aging). The impact of high air humidity can be clarified with Fig. 2; the air part under the finger will be filled (partly) with water, resulting in scattered reflection.

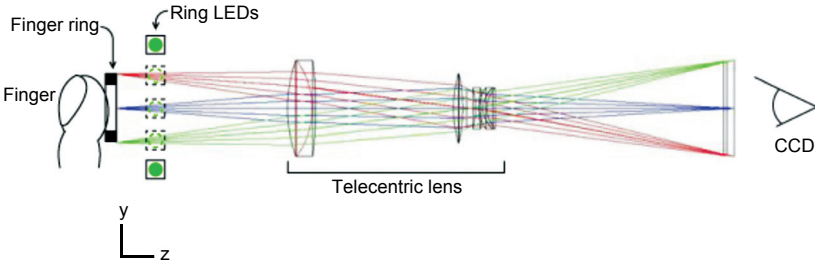

Fig. 2. Optical layout of the sensor.

2. Inconsistent contact; to be determined by the contact of the finger on the glass plate. On the glass plate the original (three-dimensional) shape of the finger gets mapped into the two-dimensional surface. Furthermore, there is no precise control of the exact position on the sensor, as each impression of a finger may possibly depict a different portion of its surface.

3. Variations in pressure on the glass plate; this will result in elastic distortions of the friction skin of the finger. The mechanical properties of the skin, determined by the non linear stress/strain relationship, preconditioning, hysteresis and anisotropy, strain rate dependency, creep response and humidity play a major role in the distortion of the human skin.

4. Irreproducible contact: accidents, specific manual work may inflict injuries to the finger, which will result in changes in the ridge structure of the finger either permanently or semi-permanently. This may introduce additional fingerprint features. If these are permanent, it may be advantageous (specific unique, easy to identify, features).

3. Required surface and scanning resolution

The choice of the required surface is dependent on the specific requirements of the system, in particular the false acceptance rate (FAR) and the false rejection

rate (FRR). A false accept (impostor) occurs when an unauthorized user is identified as an authorized user and is therefore accepted by the system. A false reject (genuine individual) occurs when an authorized user is not recognized as such and is rejected by the system. STOSZ and ALYEA [13] showed in his study that surfaces for level 3 analyses of 5 mm × 5 mm to maximum 7 mm × 7 mm are sufficient. A pinhole with a diameter of approximately 7 mm is used to obtain the minimum required 5 mm × 5 mm surface. Basically, the required resolution is completely based on the applied level of detection. At level 1 and level 2, verification is related to the pattern of the image and the minutiae only. In general, a scanning resolution ($R_{\text{level 1}} = R_{\text{level 2}}$) of 500 dpi is sufficient. This is equivalent to almost 20 dots (points) per mm [ppmm]. At level 3, a significant higher resolution is required as pores should be distinguished as well. Pores have various (unique) shapes and have a cross-section varying from 60 μm–220 μm (average 109 μm). Ridges vary in width between 100 μm–400 μm, the depth varies between 75 μm–200 μm. Generally, the period of a ridge/valley cycle is about 500 μm. With the ring diameter of approximately 7 mm, there are approximately 14 ridges across an image, which certainly results in more than 15 minutia points per image. The amount of pores per square inch is approximately 2700–3500 (equivalent to 4.19 to 5.19 pores per mm^2), giving a pore density of approximately 5 pores per mm^2. The smallest size of a detectable pore is 60 μm. On average, there are 25.6 pores per cm ridge. If we assume a sampling period of half the size of the smallest pore (60 μm), we require a minimum resolution of the sensor of 1000/30 points (dots) per mm. This is equivalent to approximately 800 dpi (ppi).

4. Sensor design

To analyse the fingerprint ridge patterns and pores, a system is required that can produce a high resolution and good quality image of the surface of the finger. The complete hardware configuration used to acquire this image is referred to as the sensor. The sensor applied consists of the following components:

1. Ring LED illumination CCS LDR-75LA-1-GR (525 nm); the present available sensors mostly have direct light. By applying ring LEDs (light emitting diodes) strike light is obtained instead of direct light. The result is a significant higher contrast of the image between the ridges and valleys. Even more, the higher the angle of strike light on the image, the higher the contrast. In the valleys between the ridges there will be almost no light, only shadows, resulting again in a higher contrast. The higher the contrast, the better the available information of the image. The distance between the finger and the light source is chosen empirically, in order to obtain the best contrast. Figure 3 shows that, with this angle of strike light, there will be no direct light in the valleys. That light will be reflected diffusely, so only a part, although sufficient, of that light will reach the camera.

The choice of a different spectrum (standard; white light) is also a unique additional feature. It is related to the penetration level of the light into the skin, in order to obtain the maximum reflection. Green light has a relative low penetration depth. This low

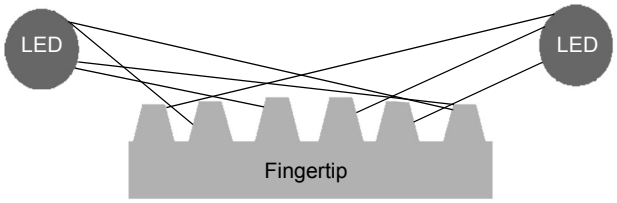

Fig. 3. Example of the high angle of strike light by the green ring LED's, showing almost no light in the valleys.

penetration depth ensures that only the surface of the finger is observed, instead of the finger tissue. For instance, with a low power red light (5 mW), almost all light will go through the finger. An UV light source seems ideal, but is harmful for the skin after intensive usage. Later in this paragraph, this relation will be highlighted. The lower the wavelength, the better the reflection. However, a (financial) trade off has to be made as well. At the time of the building of our prototype, green light was the "best" available source. At the moment of writing, blue LEDs are becoming available for attractive prices. Another, not negligible, advantage of green light is the fact that this wavelength is in the middle of the visible spectrum, ideal for camera lenses. Camera lenses are optimized for the total visible spectrum. Therefore, in general, the applied lenses have the best resolution and no achromatic aberrations in the green spectrum area.

2. Telecentric lens Jenatech JENmetar 0.7x/12. The choice for this specific telecentric lens is supported by the following arguments:

– By applying all kinds of fingers (sizes), a small distortion of the finger on the ring holder will certainly occur. A telecentric objective certifies the same magnification when these small distance variations (in *z*-direction) occur. The image distance is 100mm.

– The range of telecentricity is 7.5 mm, the depth of focus (50 μm) is 1.0 mm and the magnification is 1.4. This magnification is chosen to image the desired diameter of 7 mm finger surface on the CCD camera. Furthermore, the image quality of the lens is higher than the required quality of the camera. The telecentric lens consists of 4 components.

– The field curvature of these telecentric lenses is almost negligible (27 μm, ref. Figure 6). Again, in practice, the positioning of the finger on the ring will never be exactly the same. It is possible, however, to reduce this drawback to its maximum by applying specific ergonomics. An ergonomic design with almost no play in the position of the finger will give improved results.

3. CCD camera Sony XCST51CE. The camera is chosen based on the required image size and resolution, naturally in combination with the applied lenses. The camera is a standard CCD camera with a 1/2 inch chip comprising 752×582 pixels with 8 bits/pixel. The size of a pixel is 8.6×8.3 μm. At a 1 to 1 magnification, the image of 50% of the smallest detail (a pore of 60 μm) is approximately 3.6×3.5 pixels (30/8.3×30/8.6). The spatial resolution (sampling rate) is approximately 120 ppmm

(≈3000 ppi) in the horizontal direction and 116 ppmm (≈2900 ppi) in the vertical direction. This is 3.75 times greater than the required resolution of the sensor. The sensor itself provides approximately 1.6 (800 ppi/500 ppi) times greater resolution than those conforming to the FBI's current automated fingerprint identification system (AFIS) nominal specifications of 19.7 ppmm (500 ppi). The choice for a black and white camera is based on the limited wavelength spectrum. Applying a monochrome camera, a higher resolution can be obtained. The speed of the camera is not important, as the finger will be steadily positioned on the ring holder.

4. Ring holder for positioning of the finger. To assure that the position of the finger is almost similar at all circumstances, the choice is made for a ring (kind of pinhole) with an inner diameter of approximately 7 mm. Furthermore a ring has a substantial advantage to a standard (glass) device (mostly prisms), as:

– There are no reflections at the measurement surface;
– No dirt will influence the measurements;
– No damage to the measurement surface;
– Even light contrast over the obtained image (at a glass plate the finger is pressed more firmly at the centre).

The whole layout is mounted on an optical table. By applying a black cardboard cover, the whole set-up is protected against scattered light from the surroundings.

5. Position of the components

To explain the position of the components, the optical layout according to Fig. 2 will be used.

This figure shows the actual layout. The finger is positioned by means of the ring holder in the object surface of the telecentric lens (left end). The ring LEDs are positioned approximately 20 mm from the ring holder in the direction of the telecentric objective. The telecentric lens, next to the ring holder, consists of a doublet lens, followed by a biconvex lens, a single concave lens and again a doublet lens. Finally, on the right side of the layout is the chip of the camera. The reflected light on the finger is reflected through the opening of the ring LEDs and travels trough the telecentric lenses to the CCD chip of the camera, which is mounted directly on the telecentric lens. The three spots in the camera (right end) are examined by a spot diagram, according to Fig. 4. This figure shows clearly that all spots are within the diffraction limit.

6. Simulation

The graph representing the spot diagram of the light spots (different wavelengths) into the CCD of the camera is a typical example of required characteristics to determine and check the performance of the components of the final layout of the sensor.

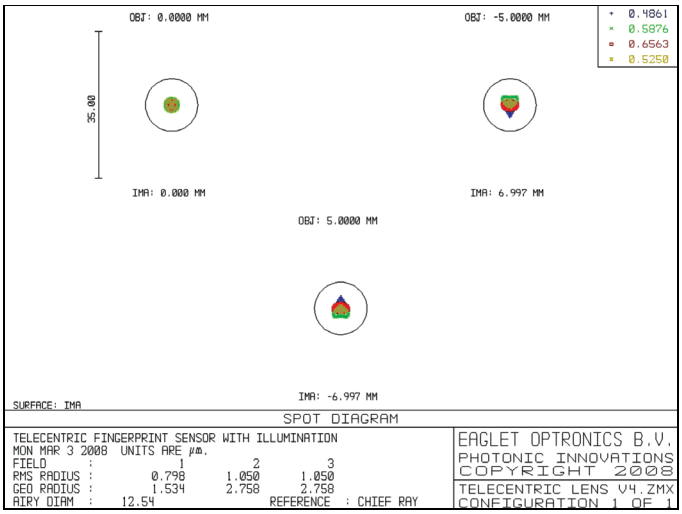

Fig. 4. Spot diagram of the light spots into the CCD of the camera.

The characteristic of the complete system (and its components) is determined by simulation by the worldwide used optical design software program Zemax. By measuring the contrast in the image plane, due to sinusoidal objects of varying the spatial frequency, the modulation transfer function (MTF) of an optical system is determined. The simulation test results are used to further improve the complete system. The only limitations are the physical boundaries of the components. Applying above described Zemax simulation program, the next step is to specify the Seidel aberrations of the applied lenses. Finally, the magnification of the telecentric lens, the depth of field, the spot resolution and the (spread of) illumination of the led light on the finger should be analysed.

7. Seidel aberrations

Whatever system used, there will be always aberrations in an optical system, similar to noise in the electronics of the camera. The objective is to minimise these aberrations. To determine which parameters are important, the functionality of the sensor should be considered. The system should be used for fingerprint verification in ATM's. Most important are the differences in person's finger sizes and the environmental conditions. The position of the finger will vary due to these significant differences in sizes.

This positioning inaccuracy should be compensated. The ergonomically design will contribute, but the system should cope with a positioning inaccuracy of approximately ±1 mm. This implies that the deviations in the image should be the same over the complete image field. Environmental conditions also have an impact on finger

sizes. All available aberrations are discussed below. Since only one wavelength (525 nm) is used, only monochromatic aberrations are considered.

7.1. Lens field flatness (field curvature)

Almost all lens systems experience field curvature. The image of a flat object will have a curved image. Field curvature is even applicable on thin lenses. The displacement Δx of an image point at height y_i on the Petzval surface from the paraxial image plane (Fig. 5) is given by:

$$\Delta x = \frac{y_i^2}{2} \sum_{j=1}^{m} \frac{1}{n_j f_j} \tag{1}$$

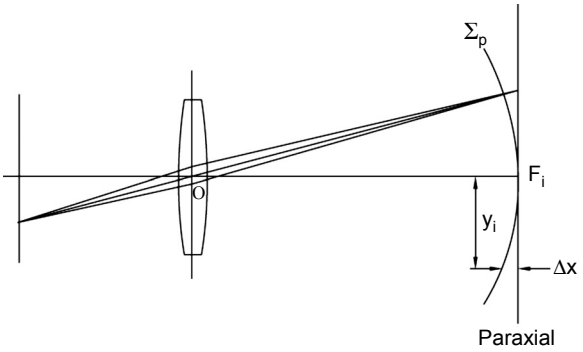

Fig. 5. Field curvature (copy Hecht, page 228 [3]).

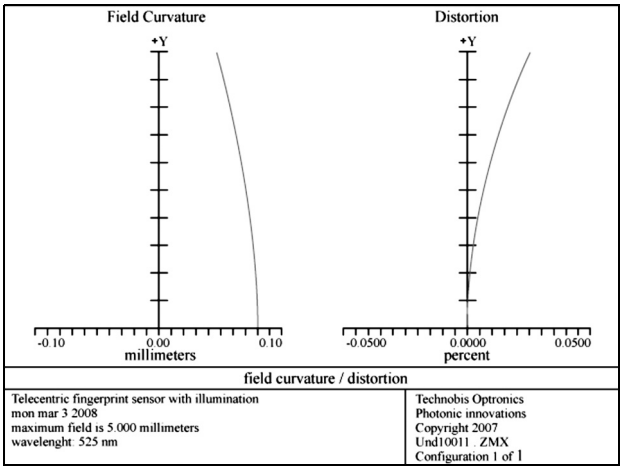

Fig. 6. Field curvature and distortion of the sensor system (525 nm only).

where n_j and f_j are the indices and local lengths of total number m of thin lenses forming the system. The shift Δx of the image point with respect to the optical axis is called "sagital".

The field curvature as calculated by the Zemax simulation program is presented in Figure 6.

7.2. Lens distortions

Distortion is the transversal opposite of the field curvature. If a grid of straight lines is projected through a lens system with distortion, the image will show curvatures.

Figure 7 shows that there is no distortion in the middle of the lens field. The distortion will increase slightly towards the edges of the lens field.

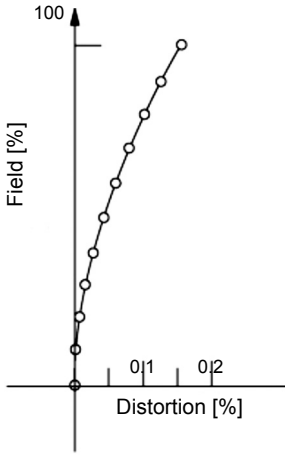

Fig. 7. Distortion versus lens field.

By decreasing the lens field, the required distortion can be obtained. However, the reduced field should contain sufficient information. A high degree of distortion makes the measurement very sensitive to positioning. Especially in our research this is very important, as the measurements are not only containing information in the centre of the image.

The whole detected area contains information, all with the same degree of importance. Images with a distortion less than 1% cannot be detected by human eye. In general, telecentric lenses have a low distortion, which supports the choice for the layout.

Initially, with the choice of the components, it was known that a light form of distortion could be solved by writing a relative simple software routine to correct the distortion anomalies at the edges of the finger ring. A disadvantage, however, is the additional calculation time for the final verification. The Zemax simulation below shows the percentage of distortion as function of the distance from the optical axis (Fig. 6).

This figure shows both the field curvature and the distortion of the sensor layout in one graph. The first part shows the shift Δ, called "sagital" (S) as function of the distance to the optical axis. It clearly shows that the field curvature of the sensor system is low, maximum 0.027 mm (27 μm). This can be neglected. The distortion, also as function of the distance from the optical axis, is also negligible (as expected), less than 0.018% at the outer edge of the finger ring. Conclusion: the field curvature and the distortion of the sensor are negligible.

7.3. Spherical aberration

This will occur by focussing a parallel beam by a single lens. As the beam hits the lens farther from the axis, the focus point will be nearer to the lens. The magnitude of the aberration highly depends on the orientation of the lens. Applying a focussing lens with the flat surface towards the focus point, will reduce this to almost zero, as applied in our set-up. Spherical aberrations can therefore be neglected.

7.4. Coma

By applying a symmetrical optical system, the form of the wave front will depend only on the aperture angle and the field angle. The magnitude of coma is proportional to the field angle. In our case this field angle is almost zero. Therefore, coma can be neglected.

7.5. Astigmatism

When the light beam hits the lens under an angle, one part of the light beam will travel a shorter distance than the other part of the beam. The result is a distorted beam with an elliptical shape. The focuses in both directions are (slightly) differently positioned. Again, the (field) angle is almost zero. Astigmatism can be neglected as well.

Coma, spherical aberrations and astigmatism are present in every image point of the system and depend on the position in the image field, different dimensions will occur. As a result of this, the object point, in principle very small, will be imaged as a spot with a certain dimension. As long as these images are smaller than one pixel of the camera, these object points are perfect to distinguish. The MTF analysis is doing the same. These aberrations analysis is only to be used for the designer, to determine which components should be altered.

7.6. Magnification

To distinguish details in an image, the detail should be minimum 1 pixel. As stated earlier, due to noise and the fact that not every object can be imaged with one pixel, we assume a minimum required amount of 4 pixels (2×2). Without magnification we have to distinguish minimum a half pore (30 μm), thus 3.6×3.5 pixels are required. This would require a magnification of approximately 1.7–1.8. However, the sharpness of the image should be sufficient. The modulated transfer function (MTF) gives an excellent indication how a point of the object is imaged on the CCD camera (spot

diagram). By applying a magnification, it will be possible to enlarge, and thus clarify, the smaller details, providing the image quality of the lens is sufficient. When the resolution of the lens is too low, the image will "mix" over a number of pixels. For this research, a magnification factor of 1.4 is chosen. Experimentally, it turned out to give the best results, a slightly higher magnification showed image quality loss.

7.7. Depth of field

The finger is three dimensional and is converted to a two dimensional image. However, the relief (depth) in the finger skin is the basis for the fingerprint. To analyse this profile (ridges and pores), it is vital that the object is imaged sharp over a certain distance. It is obvious that it is impossible to put the finger always exactly at the same position. The fingers differ in size, which causes a depth difference in putting the finger on the ring. Furthermore, the ridge depths per person may differ significantly. These positioning differences have to be compensated with a depth of field of several millimetres. The depth of field can be adjusted by changing the numerical aperture (NA). These are inverse related. One should realise, however, that increasing the NA, the resolution (detail value) will decrease by the following formula:

$$S = \frac{\lambda}{\mathrm{NA}} \tag{2}$$

where S is the detail value (in our case the object size, half the minimum pore size, thus 30 μm) and λ – the wavelength. The NA of a lens system is determined by:

$$\mathrm{NA} = n \sin\theta \tag{3}$$

where n is the refractive index and θ – half the opening angle. There should be a trade-off between the acceptable depth of field and the required detail value. By running the Zemax simulation we can perform a through focus analysis, by measuring the spot diameter at different distances. The start (zero) position is the middle of the focus point; everything is perfect aligned on the optical axis of the sensor system. To have an indication of the impact of the depth of field, the distance between the finger and the chip of the camera is shifted in two steps of ±5 mm (thus in total 10 mm). This covers the surface range of the chip of the camera (1/2 inch), as the radius will cover the edges of the chip.

Furthermore, there is a shift of focus assumed in steps of ±150 μm to a maximum of ±300 μm. Figure 8 shows the spot diameter fluctuations by these extreme shifts. As the system was optimized and tested for the complete visible RGB spectrum, some specific wavelength are depicted. The green curves are for a wavelength of 500 nm (nearest to the 525 nm applied LEDs). To ascertain that the maximum fluctuations in shift of the finger are still in focus (thus a good image), the shifts in focus over the distance shift of the finger should be within the airy disc diameter of the designed sensor. The airy disc diameter of the sensor is 17.93 μm, as tabled in the figure.

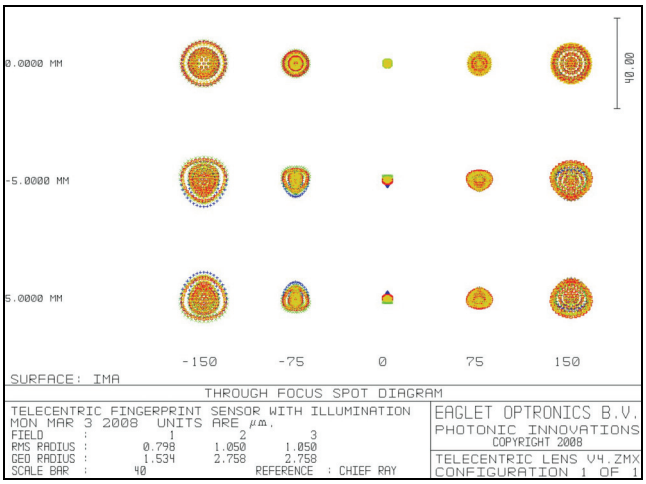

Fig. 8. Through focus spot diagram.

The tabled RMS radius and Geo radius are the spot diameters on the optical axis at the three out of focus points. The figure shows that in all circumstances (shifts in both focus and with the finger) the spots are within the airy disc diameter and therefore the image is not sensitive to the shifts.

7.8. Vignetting

As lenses are restricted in their diameter, the beam that enters the objective at an angle with the optical axis may miss a part (or the whole) of the second lens. This phenomenon is called vignetting. Due to vignetting, the contrast at the edge of the image will be lower than at the centre. The level of vignetting is dependent on the (optical) design. In general, telecentric lenses do not show a high level of vignetting, contrary to wide angle lenses.

It can be concluded that the image of the finger is still sharp with a shift of the finger over a distance of maximum 10 mm (±5 mm) and an out of focus shift of maximum 600 μm (±300 μm). The applied magnification is correct; simulations with a higher magnification show image loss. Spherical aberrations, coma and astigmatism can be neglected, as well as vignetting.

8. Modulation transfer function

Traditionally, the quality of an optical component or system was evaluated by its resolution. The better the resolution, the better the system. According to HECHT [3] the object can be represented as a collection of point sources, each of which is imaged as a point spread function by the optical system. We can now consider the object (finger) to be the source of an input lightwave, made up of plane waves. These input waves travel in specific directions corresponding to particular values of spatial

frequency. The image contrast C or modulation at a given resolution should be determined. The higher the contrast, the better the specific details of the images. The resolution is expressed as a percentage of the number of line pairs per millimetre. The quality of the image can be determined by measuring the contrast of a number of line pairs of the obtained image. When $I_{\max}$ is the maximum irradiance value of the image and $I_{\min}$ is the minimum irradiance value, the contrast C is calculated as follows:

$$C = \frac{I_{\max} - I_{\min}}{I_{\max} + I_{\min}} \times 100\% \tag{4}$$

When in the image the black lines are real black ($I_{\min} = 0$) and the white lines are real white ($I_{\max} = 1$), then the contrast is maximum, 100%. When the lines are close to each other, the contrast will decrease. In general, there will be an output loss. This can be expressed by the modulation transfer function (MTF), defined as the ratio of the image modulation to the object modulation at all spatial frequencies. The MTF of an optical system is determined by measuring the contrast C in the image plane, due to sinusoidal objects of varying the spatial frequency.

The maximum MTF of a system will be determined by the diffraction limit. Light has a natural diffraction, which causes that the spot diameter never could be smaller than half the wavelength. The diffraction limit d is determined by the following equation:

$$d = 1.22 \frac{f}{a} \lambda \tag{5}$$

where λ is the wavelength, f – the focus length of the lens and a – the diameter of the light beam on the lens; a can also be the diameter of the lens when the light beam covers the complete lens. Applying the above to the chosen sensor system, the sensor requirements and limitations should be considered. The smallest required detail is 30 μm (half the smallest pore diameter). Both the camera and the telecentric lens have a MTF. The actual MTF of the system is determined by the lowest MTF. The MTF of the camera is the limiting factor. The MTF of the camera is determined by the size of the pixels. The camera is a VGA camera with 752×582 pixels (equivalent to 8.6 μm×8.3 μm). To distinguish a pair of lines, a minimum of two pixels is required. Taking the smallest size of 8.3 μm, the maximum spatial frequency in cycles per millimetre is (LPM is line pairs per millimetre):

$$\frac{1000}{8.3 \times 2} = 60.2\text{LPM} \tag{6}$$

This is the maximum camera resolution. In the calculations it is assumed that the pixels have a maximum contrast. The question is: will the sensor system have a sufficient contrast ratio at the 60.2 line pairs per millimetre? Literature shows that

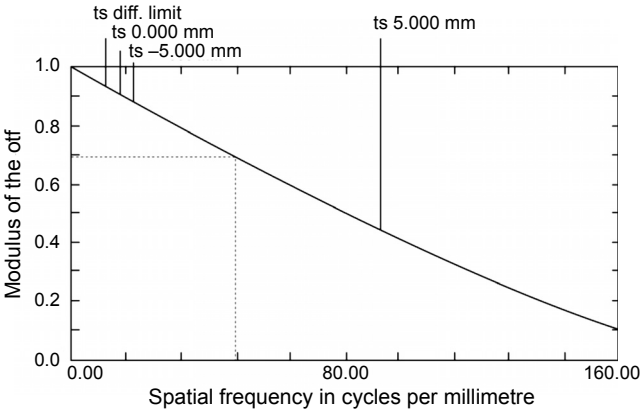

Fig. 9. MTF graph of the telecentric lens of the fingerprint sensor.

a minimum of 20% contrast ratio is required still to distinguish the pair lines [3]. The fingerprint system lenses should have at 60.2 line pairs per millimetre a minimum contrast ratio of 20%. The MTF of the telecentric lens is shown in Fig. 9.

The figure shows that at the spatial frequency of approximately 60 pair lines per millimetre there is a contrast of approximately 0.69 (equivalent to the contrast ratio of 69%). This exceeds the required minimum contrast ratio of 20% and therefore suffices the system requirements. We can therefore conclude that the system, with the chosen lens systems (telecentric lens), and the attached camera have both the required MTF to obtain a sufficient contrast to distinguish the minimum size of a pore ($1/2 \times 60$ μm), required for level 3 classification.

9. Light distribution over the finger

The relative light distribution (illumination) on the chip of the camera was simulated. It shows that almost 99% of the light hits the centre of the camera chip and that at the edges there is still 95% illumination observed. The illumination yield over the *x*-axis [mm] was measured from the centre of the camera chip in one direction towards the edge. As the sensor system is rotational symmetric, the light distribution on the chip is in all directions the same. One can conclude that an illumination loss of approximately 3–4% over the whole camera chip is negligible. There is thus almost no vignetting.

It has been shown that there is almost no contrast loss towards the edges of the lenses. In almost all used techniques, the light source is a single point source, in some cases extended with an additional light source. Here we obtain our unique feature, applying ring LEDs, resulting in a light distribution over the finger that is almost evenly distributed. The sensor layout shows the application of the ring LEDs. The light distribution of the ring LEDs is quite even, but not perfect. The next graphs (Figs. 10 and 11) show the distribution of light over the finger, the left graph as a cross-section and the right graph actually on the finger.

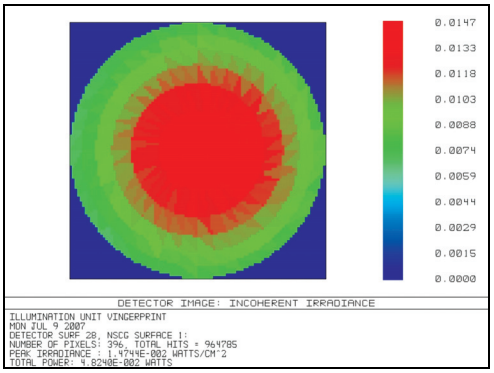

Fig. 10. Light distribution over the finger.

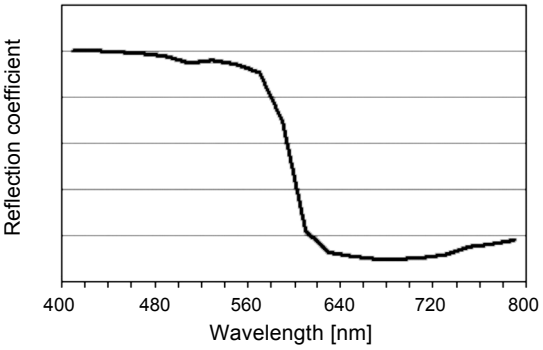

Fig. 11. Reflection in the skin as function of the wavelength.

On the left side (red surface) of Fig. 12 the finger is positioned. The graph clearly shows that the finger is not flat. The right cross-section is the ring led. It is noted that not all beams from the LEDs do hit the finger, as a percentage of the light is lost. These lost beams are cut of in the graph by the software program. As the finger is not flat (it is positioned on an open ring), the actual illumination on the finger [watt/cm^2] follows the above distribution. The power loss of almost 50% from the core to the edges has obviously an impact on the contrast loss (Fig. 10). However, the obtained simulation results and the actual images show sufficient contrast, mainly due to the reflection obtained by using strike light (Fig. 3). To eliminate this, more LEDs

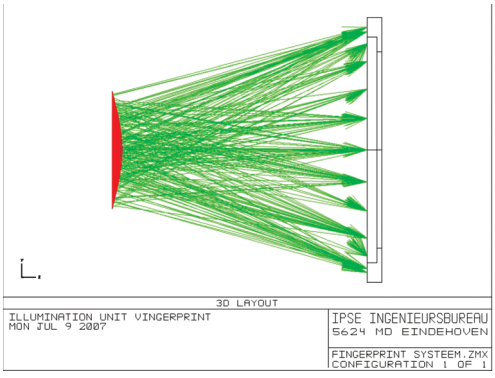

Fig. 12. Cross-section light distribution over the finger.

could be used or higher out put power should be: to improve the contrast, more LEDs could be used or LEDs with a higher output power. Furthermore a higher reflection on the skin (thus a higher contrast) could be obtained by using a lower wavelength (*e.g.*, blue LEDs), according to Fig. 11.

9.1. Penetration depth of light in the human skin

To obtain the maximum reflection of the light on the finger, one should know the relationship of light reflection on the skin as function of the wavelength. The combination of the ring led light distribution and the chosen light wavelength for fingerprint applications is unique. The skin is permeable to light between approximately 600 nm and 1100 nm. Basically the penetration depth of the human skin as function of the wavelength is a standard graph (ref. [14]). This is referred to as the "optical window" for tissue. The depth of penetration of the incident light into tissue is directly proportional to the wavelength. The longer wavelengths penetrate more deeply and therefore the higher percentage of light will be transmitted. The mentioned applications seem reverse we seek the maximum reflection instead of possible penetration. Figure 11 shows the reflection of the skin as function of the wavelength.

The graph is obtained by applying a wavelength λ dependent reflection κ as function of the "standard" penetration depth Z_p, defined as:

$$\kappa = \frac{\lambda}{4\pi Z_p} \tag{7}$$

It shows that the applied ring LEDs (525 nm) have a good reflection, significantly better than the standard applied light sources. The essence of the penetration value is evident, since any penetration in the skin will result in a lower contrast of the obtained image. We have chosen the relatively cheap 525 nm (green) LEDs at the time of building the system. The development in LEDs is enormous and it is possible now to purchase LEDs with a lower wavelength for the same price. It is therefore recommended to use UV LEDs with a wavelength just under 400 nm. The figure shows that indeed substantial improvement can be gained.

10. Test result images

Numerous images have been made with the designed prototype, showing good results. In all cases pore features have been observed and all images could be used for imaging processing, required for the performance analysis of the sensor. It was noted that there is a significant difference in the obtained image results between fingers with a dry skin and sweaty fingers. Figure 13 below shows some examples of the test images. Among them, images from the fingers of the author.

With these results several imaging processing techniques have been applied in order to determine the system performance of the sensor, *i.e.*, the feature (pores) uniqueness expressed as the false acceptance rate (FAR) and the feature (pores) and algorithm reliability, expressed as the false rejection rate (FRR). The match score S_F

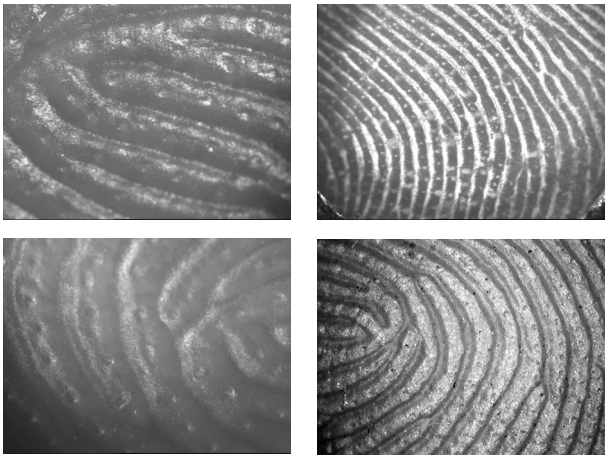

Fig. 13. Test result images from the sensor prototype.

or performance of a system is defined in terms of the number of false accepts and false reject errors, in order to compare the detected features (pores) in the original template and the live scan. It can be expressed by:

$$S_F = \frac{n_m}{n_1} - \frac{n_2 - n_m}{n_{2,\max}} \tag{8}$$

where n_1 – the true number of features in the template (segment 1), n_2 – the number of features detected in the live scan (segment 2), $n_{2,\max}$ – the maximum number of features allowed in the live scan (segment 2, assume equal to n_2), n_m – the number of matching features.

Figure 14 below shows the final error rate plot of the sensor system. It should be noted that the FAR and FRR values at the complete match score and the complete mismatch score should be exactly –1 or +1. In reality this is not the case. The equations give values which cannot be interpreted anymore. In our case, the match scores above

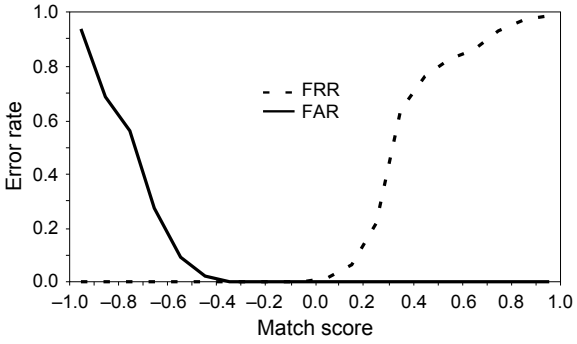

Fig. 14. Error rate (FAR and FRR) plots against match score.

±0,9 are not representative anymore. This is also not the area we are looking for. A perfect FAR will result in an unacceptable FRR.

The FAR and the FRR intercept each other at approximately 2.5×10^{-5}. This is the equal error rate (EER) point. At that point the match score is −0.1158. To compare these values with, for instance, the bank requirements, at a FRR of 0.05% (5×10^{-4}), the obtained FAR is approximately 5×10^{-6}, which is significantly (factor ≈ 1000) better than the minimum bank requirement of the FAR of 0.1% (1×10^{-3}).

11. Conclusions and recommendations

Applying ring LEDs with a low wavelength (525 nm), combined with a specific sensor set-up and layout (strike light), we have shown that pores can be detected for verification purposes. The chosen camera and the applied lens systems (telecentric lens) meet the required MTF to obtain a sufficient contrast to distinguish the minimum size of a pore for level 3 classification. The obtained contrast ratio also exceeds by far (≈70%) the minimum required contrast ratio of 20%. The field curvature of the sensor, the shift Δx, as function of the distance to the optical axis, is low, maximum 0.027 mm. This can be neglected. As expected with telecentric lenses, the distortion of the sensor is also negligible (less than 0.018%). The depth of field shows that the image of the finger is still sharp with a shift of the finger of maximum 10 mm (±5 mm) and an out of focus shift of maximum 600 μm (±300 μm). Vignetting is less than 3–4% and therefore negligible. Spherical aberration, coma and astigmatism are also negligible. The matching score, the indicator for the performance of the sensor system, shows a significant improvement to standard white light systems. It can be concluded that the unique sensor features, the light distribution and the applied wavelength to reduce the depth penetration of the light in the skin, do result in images with clear level 3 features (pores).

Due to the ongoing developments (both technically and financially) in LEDs and lasers, better results can be obtained by applying more LEDs, higher powered LEDs and a lower wavelength (*e.g.*, blue light) for a higher reflection on the skin. When additionally optical components are added, the size of the complete sensor can be compressed significantly (90 mm).

References

[1] ASHBAUGH D.R., *Poroscopy*, Identification News, November 1982 (this article was reprinted in *The Print* **11**(6), 1995, pp. 1–7).

[2] GALTON F., *Fingerprints*, London, McMillan and Co., New York, 1892.

[3] HECHT E., *Optics*, Addison-Wesley Publishing Company Inc., 1987.

[4] JACOBS R.H.R., SCHELLEKENS P.H.J., VELZEL C.H.F., BUSSELAAR E.J., *Proefopstelling Fingerline Tracking*, Afstudeerverslag, Technische Universiteit Eindhoven, Faculteit Werktuigbouwkunde, Sectie Precision Engineering, Rapportnummer PE2001-053, 2001.

[5] JAIN A.K., LIN HONG, PANKANTI S., BOLLE R., *An identity-authentication system using fingerprints*, Proceedings of the IEEE **85**(9), 1997, pp. 1365–1388.

[6] JAIN A.K., ROSS A., PRABHAKAR S., *An introduction to biometric recognition*, IEEE Transactions on Circuits and Systems for Video Technology **14**(1), 2004, pp. 4–20.
[7] JAIN A.K., PRABHAKAR S., SHAOYUN CHEN, *Combining multiple matchers for a high security fingerprint verification system*, Pattern Recognition Letters **20**(11–13), 1999, pp. 1371–1379.
[8] MAIO D., MALTONI D., *Direct gray-scale minutiae detection in fingerprints*, IEEE Transactions on Pattern Analysis and Machine Intelligence **19**(1), 1997, pp. 27–40.
[9] O'GORMAN L., NICKERSON J.V., *An approach to fingerprint filter design*, Pattern Recognition **22**(1), 1989, pp. 29–38.
[10] OSTERBURG J.W., PARTHASARATHY T., RAGHAVAN T.E.S., SCLOVE S.L., *Development of a mathematical formula for the calculation of fingerprint probabilities based on individual characteristics*, Journal of the American Statistical Association **72**(360), 1977, pp. 772–778.
[11] PANKANTI S., BOLLE R.M., JAIN A., *Biometrics: The future of identification*, Computer **33**(2), 2000, pp. 46–49.
[12] RODDY A.R., STOSZ J.D., *Fingerprint features-statistical analysis and system performance estimates*, Proceedings of the IEEE **85**(9), 1997, pp. 1390–1421.
[13] STOSZ J.D., ALYEA L.A., *Automated system for fingerprint authentication using pores and ridge structure*, Proceedings of the SPIE **2277**, 1994, pp. 210–223.
[14] VELZEL C.H.F., VAN RIJNBACH M., VAN DER VEEN J.M., *Elementary Optics*, Eaglet Optronics, 2007.
[15] http://www.medicalbiocare.com/html/advantages-technical.html – *Penetration depth of light in human skin*.

Received April 14, 2010